Supplemental Materials

Exploring the magnetic phase diagram and Hall resistivity suppression in centrosymmetric $GdOs_2Si_2$ single crystal

Hiroaki Hayashi,[1,2,*] Moyu Kato,[3] Taichi Terashima,[1] Naoki Kikugawa,[4] Hiroya Sakurai,[1] Hiroyuki K. Yoshida,[3] Kazunari Yamaura [1,2]

[1] Research Center for Materials Nanoarchitectonics, National Institute for Materials Science, 1-1 Namiki, Tsukuba, Ibaraki 305-0044, Japan

[2] Graduate School of Chemical Sciences and Engineering, Hokkaido University, North 10 West 8, Kita-ku, Sapporo, Hokkaido 060-0810, Japan

[3] Department of Physics, Hokkaido University, North 10 West 8, Kita-ku, Sapporo, Hokkaido 060-0810, Japan

[4] Research Center for Energy and Environmental Materials, National Institute for Materials Science, 3-13 Sakura, Tsukuba, Ibaraki 305-0003, Japan

*E-mail: hhayashi@issp.u-tokyo.ac.jp

Magnetic susceptibility over a wide temperature range:

Additional data for magnetic susceptibility over a wide temperature range is presented in Fig. S1, depicting the χ-T curves for $\mu_0 H$ = 1 T with H//[100], [110], and [001]. Each curve displays Curie-Weiss behavior at higher temperatures, and a distinctive peak at T_1 = 26.6 K signifies the antiferromagnetic ordering of the Gd^{3+} moments. The Curie constant (C) and Weiss temperature (Θ_w) were determined by analyzing the linear temperature dependence of the inverse magnetic susceptibility above 100 K. For H//[100] and H//[110], C was calculated to be 8.39(1) emu K mol^{-1} with Θ_w of +24.9(1) K, while for H//[001], C was found to be 8.20(1) emu K mol^{-1} with Θ_w of +25.4(5) K. The calculated effective magnetic moment derived from the Curie constant was 8.19(1) μ_B for H//[100] and [110], and 8.01(1) μ_B for H//[001]. These values slightly exceed the theoretical value of μ_{eff} = 7.94 μ_B for Gd^{3+} ions, suggesting a well-localized nature of the 4*f* electrons of Gd^{3+} ions, with the itinerant 5*d* electrons of Os ions contributing to the spin moment [43]. Despite the antiferromagnetic ordering, analogous to $GdRu_2Si_2$ [26,27], the dominant interaction between Gd^{3+} moments is considered to be ferromagnetic due to the positive Weiss temperature. Moreover, while the paramagnetic state is nearly isotropic, the magnetic susceptibility below T_1 is highly anisotropic, notably with the susceptibility for H//[001] significantly lower than that for H//[100] or [110]. This observation suggests that the Gd^{3+} moments are ordered along the c-axis, in line with the magnetic structure of $GdRu_2Si_2$ [24].

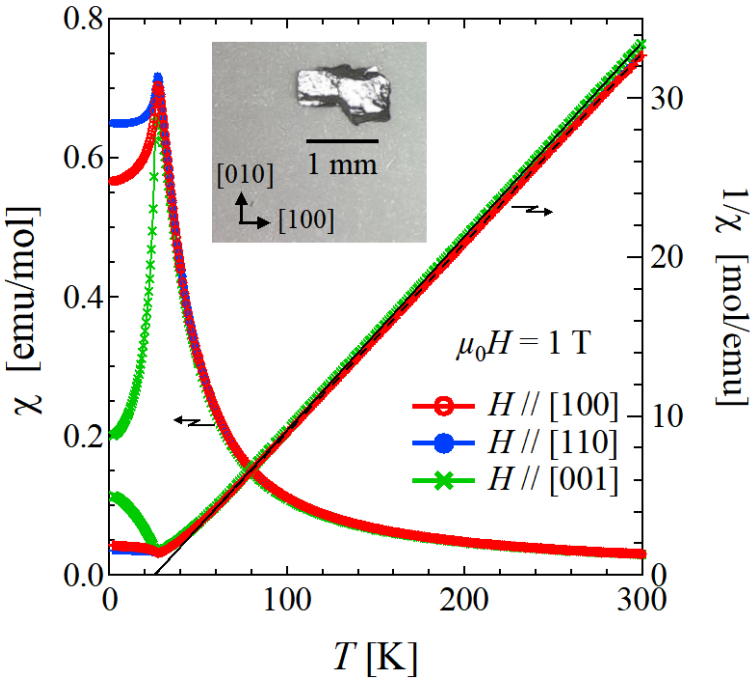

Fig. S1: Temperature dependence of magnetic susceptibility under a magnetic field of 1 T along [100], [110], and [001]. The solid black line represents the Curie-Weiss fitting. The inset shows the crystal structure of $GdOs_2Si_2$ [35]. The inset is a photograph of the centrosymmetric $GdOs_2Si_2$ single crystal. All measurements were carried out using the single crystal shown in this photograph.

Supplemental Hall conductivity data:

Additional data for Hall conductivity are determined using the equation $\sigma_{yx} = -\rho_{yx} / (\rho_{xx}^2 + \rho_{yx}^2)$ as presented in Fig. S2. The σ_{yx} increases linearly up to H_1, whereas the hump-like enhancement is identified in phase II. This enhancement is completely suppressed in phase II', leading to broad peak in phase III.

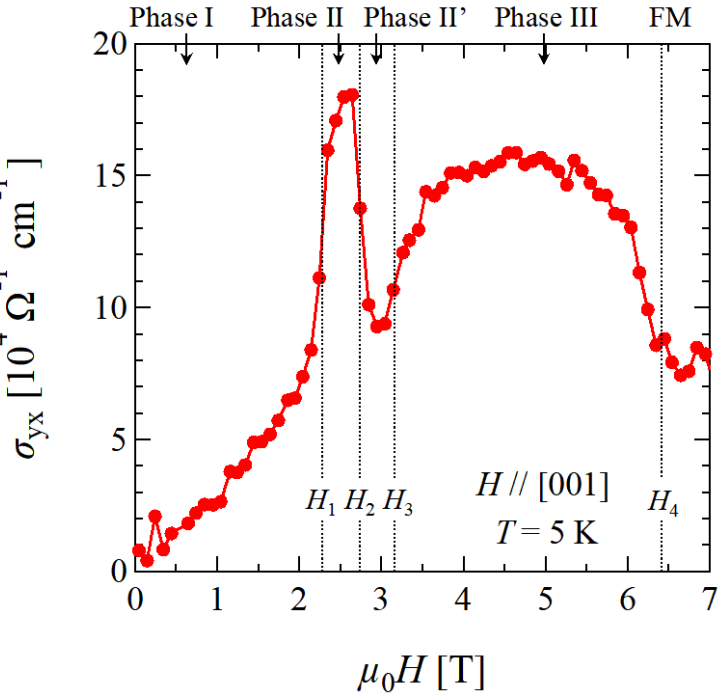

Fig. S2: Magnetic field dependence of σ_{yx} at 5 K for H//[001]. The gray and yellow regions correspond to the phases II and II', respectively.

Supplemental Hall resistivity analysis:

We fitted the magnetic field dependence of Hall resistivity data (ρ_{yx}) along with magnetization (M) and longitudinal resistivity (ρ_{xx}) curves, as shown in Fig. S3. The calculated anomalous Hall component, ρ_{yx}^{A}, assuming intrinsic ($\propto M\rho_{xx}^{2}$) and extrinsic ($\propto M\rho_{xx}$) mechanisms, is plotted in the bottom panel of Fig. S3. As mentioned in the main text, adequate fitting could not be achieved; this analysis considers scattering of conduction electrons by relatively larger single skyrmions, whereas a short-period skyrmion lattice with smaller diameters is predicted in $GdOs_2Si_2$. The band folding resulting from the periodicity of the skyrmion lattice may contribute to increased resistivity. Therefore, a more appropriate approach is needed for analyzing the topological Hall effect.

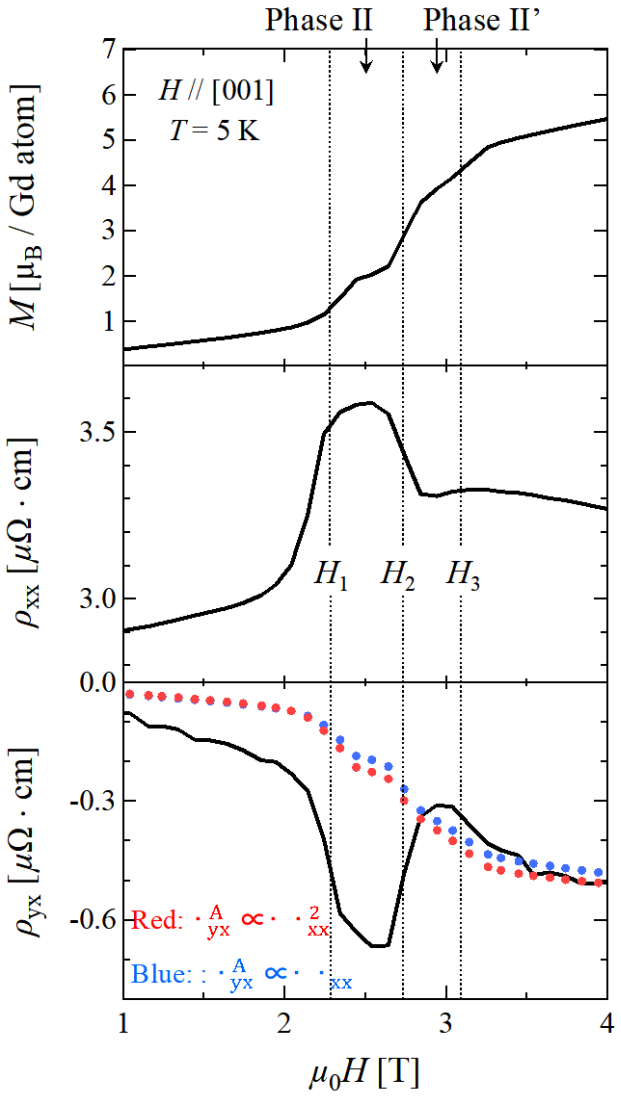

Fig. S3: Magnetic field dependence of magnetization (M), longitudinal resistivity (ρ_{xx}), and Hall resistivity (ρ_{yx}). The red and blue dots represent the anomalous Hall term calculated assuming intrinsic ($\rho_{yx}^{A} \propto M\rho_{xx}^{2}$) and extrinsic ($\rho_{yx}^{A} \propto M\rho_{xx}$) mechanisms, respectively.

Supplemental electrical resistivity data:

Additional data for electrical resistivity are presented in Fig. S3. The ρ_{xx} vs T curves exhibit anomalies at characteristic temperatures of T_1, T_2, and T_3, which correspond to the temperatures determined in the magnetization measurements. At $\mu_0 H = 0$ and 1 T, ρ_{xx} decreases as the temperature is lowered below T_1. However, at $\mu_0 H \geq 2$ T, a significant change in the temperature dependence of ρ_{xx} is observed. Specifically, at $\mu_0 H = 2$ T, ρ_{xx} experiences an abrupt increase near T_2 during cooling, followed by a subsequent decrease with further cooling. For $\mu_0 H \geq 2.4$ T, ρ_{xx} shows a weak kink at T_1 and a subsequent slight increase, followed by a further increase below T_2. Interestingly, as shown in the inset of Fig. S3, a negative magnetoresistance is observed not only below T_1 but also at high temperatures, specifically below 40 K. This finding suggests the presence of the magnetic precursor effect, a phenomenon observed in isostructural Gd-based compounds [40,41].

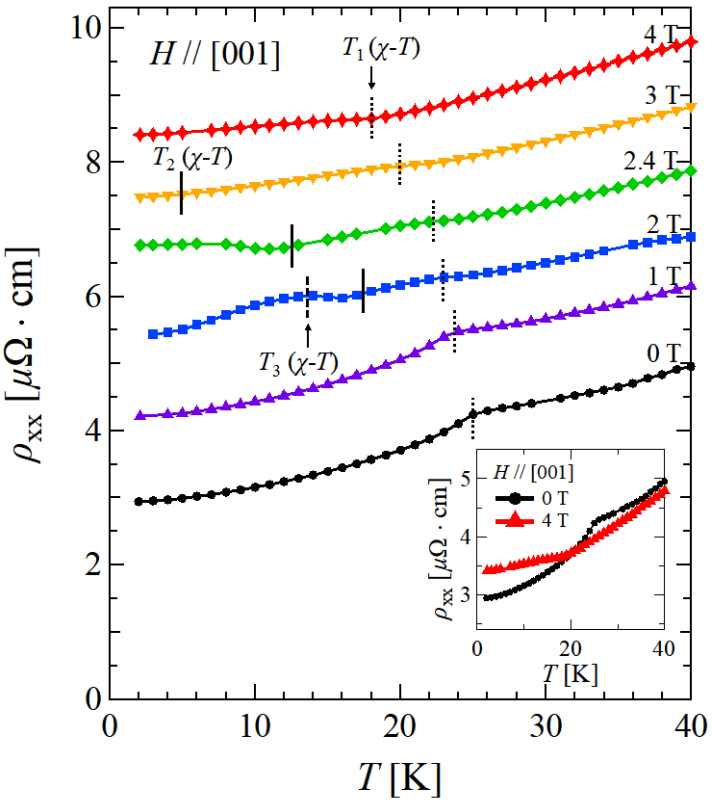

Fig. S4: Temperature dependence of the ρ_{xx} under different magnetic fields. Dotted, solid, and dashed lines denote the characteristic temperatures T_1, T_2 and T_3, respectively, determined from χ-T measurements. The data have been shifted for clarity. The inset presents ρ_{xx}-T curves at $\mu_0 H = 0$ T (black) and 4 T (red) without any offset.

Supplemental C_p data:

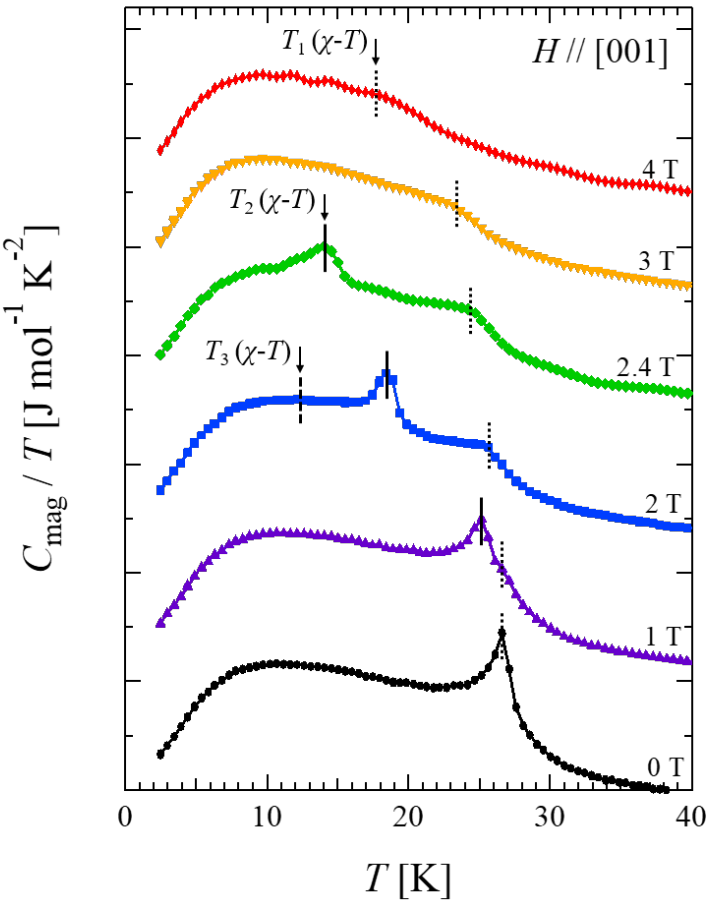

Fig. S5: Temperature dependence of C_p below 40 K under various magnetic fields. The magnetic transition temperatures at T_1, T_2, and T_3 determined from χ-T measurements are indicated by dotted, solid, and dashed lines, respectively. The data have been shifted for clarity.

Phase diagram obtained from an alternate crystal:

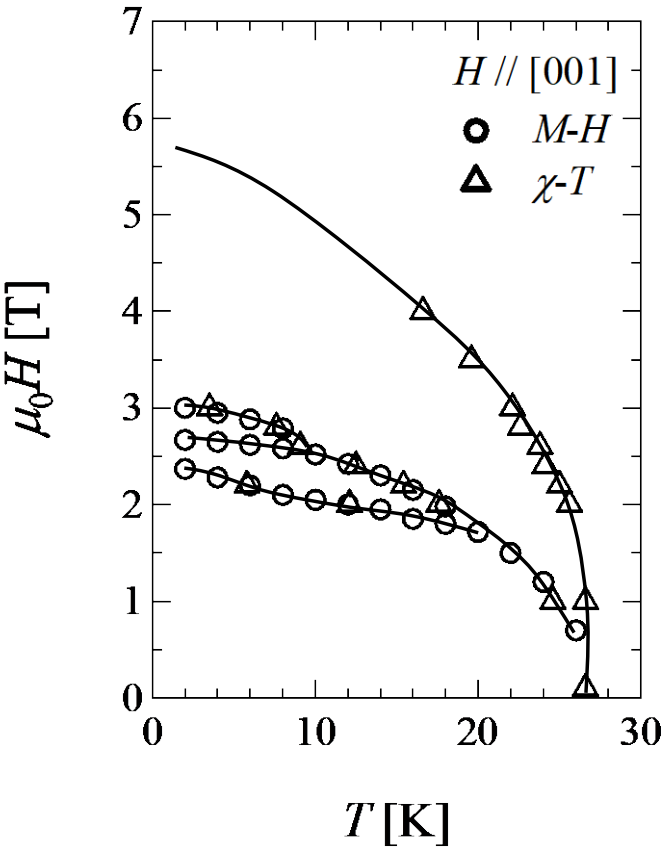

Fig. S6: Phase diagram obtained from an alternate crystal of $GdOs_2Si_2$ for *H//*[001]. Circles and triangles represent the characteristic points observed in *M-H* and χ-*T* measurements, respectively.